Water Structure in the Electrical Double Layer and the Contributions to the Total Interfacial Potential at Different Surface Charge Densities

Benjamin Rehl,[a] *Emily Ma,*[b] *Shyam Parshotam,*[a] *Emma L. DeWalt-Kerian,*[a] *Tianli Liu,*[a] *Franz M. Geiger,*[*,b] *and Julianne M. Gibbs*[*,a]

[a]Department of Chemistry, University of Alberta, Edmonton, Alberta, T6G 2G2, Canada

[b]Department of Chemistry, Northwestern University, Evanston, Illinois 60208, USA

Abstract: The electric double layer governs the processes of all charged surfaces in aqueous solutions, however elucidating the structure of the water molecules is challenging for even the most advanced spectroscopic techniques. Here, we present the individual Stern layer and diffuse layer OH stretching spectra at the silica/water interface in the presence of NaCl over a wide pH range using a combination of vibrational sum frequency generation and heterodyned second harmonic generation techniques and streaming potential measurements. We find that the Stern layer water molecules and diffuse layer water molecules respond differently to pH changes: unlike the diffuse layer, whose water molecules remain net-oriented in one direction, water molecules in the Stern layer flip their net orientation as the solution pH is reduced from basic to acidic. We obtain an experimental estimate of the non-Gouy-Chapman (Stern) potential contribution to the total potential drop across the insulator/electrolyte interface and discuss it in the context of dipolar, quadrupolar, and higher order potential contributions that vary with the observed changes in the

net orientation of water in the Stern layer. Our findings show that a purely Gouy-Chapman (Stern) view is insufficient to accurately describe the electrical double layer of aqueous interfaces.

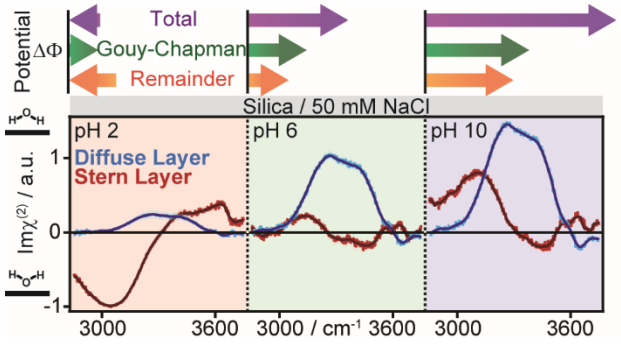

Introduction. The electrical double layer (EDL) of charged aqueous interfaces is commonly described[1-2] using theories going back to Helmholtz,[3] Gouy,[4] Chapman,[5] Stern,[6] and Grahame.[7] These mean field approximations account for the distribution of ions in close proximity to the surface and those further away in the diffuse layer, but do not explicitly include the molecular structure and chemical identity of the species comprising the EDL. Instead, these models are based on the Poisson solution for mobile, free point charges in a dielectric continuum over a uniformly charged and infinitely thin plane. Dipolar, quadrupolar, and other solvent contributions to the interactions between mobile charges in the diffuse layer are only accounted for through the use of a continuum treatment of water (as manifested in its dielectric constant, or relative permittivity). Yet for the Stern layer, increasing evidence from experiment and theory points to substantial contributions of net-aligned dipoles and higher-order moments to the total interfacial potential.[8-22] Explicit thermodynamic treatments of solvent dipoles at charged interfaces are reviewed in Habib's classic work.[23] The relative permittivity of Stern layer water is challenging to determine, with experimental estimates[24-25] ranging as low as 2 to below 30 and to a point-estimate of 43 from linear regression analyses of proton surface charge data for oxides.[26] Therefore, our current understanding of the EDL needs to be improved by considering electrostatic potential contributions beyond those captured using the relative permittivity constant of water and how such contributions evolve with changes in surface charge density. Here, we refer to such contributions as non-GCS contributions, i.e. the difference between the total potential drop across the interface and the potential drop computed using the GCS model assumptions, which employ ϵ_r to account for the properties of water. In addition, while the structure of some ions in the EDL are well understood from various measurements,[27-30] the way water molecules orient and network

themselves in its two main structural features, the Stern layer and the diffuse layer, remains enigmatic.

Strategies have evolved to address these shortcomings, such as potentiometric titrations,[29] electrical impedance measurements,[31-32] ion adsorption batch experiments,[28, 30] or electrokinetic and electrophoretic techniques,[33-34] with subsequent data interpretation employing surface complexation models.[35-36] Other methods include atomic force microscopy (AFM),[37-38] X-ray spectroscopies like X-ray standing wave and X-ray reflectivity measurements,[27, 39-40] and vibrational sum frequency generation spectroscopy.[41-43] Employing ultraflat boehmite, AFM has recently been used to report directly on the interfacial water structure[44] that constitutes the greatest component of the EDL. X-ray reflectivity and spectroscopy measurements have yielded the position of ions and hydration layers[35, 45] in the EDL for a number of different mineral oxides including mica,[46-49] titania,[35, 50] alumina,[45] and quartz.[51-52] More recently, X-ray photoelectron spectroscopy of colloidal dispersions in a microjet were used to obtain estimates for the surface potential as a function of ion concentration and identity,[27] which was used in conjunction with electrokinetic measurements to infer the thickness of the Stern layer.[53]

In contrast to important new insights from atomistic simulations regarding water orientation and polarization at oxide interfaces,[17, 54] experimental data on the orientation of water molecules, their hydrogen bonding strength, and the dipole and higher-order electrostatic contributions from the non-solvent species in the EDL (for oxides that includes the SiOH, SiO^-, positive surface sites and the interfacial ions) is still lacking. Furthermore, owing to the challenges associated with these experiments, measurements are generally performed at only one or a few pH values and a limited ionic strength range. As pH determines the surface charge density and interfacial potentials over amphoteric oxides such as silica, it would be ideal to monitor how the

structure of the EDL evolves under a range of pH conditions. Measuring the hydrogen-bonded structure of water and its absolute orientation in the Stern and the diffuse layers would provide highly complementary information to that from X-ray and scanning probe measurements, bringing us closer to the goal of generating a complete molecular picture of charged aqueous interfaces.[43, 48]

Vibrational sum frequency generation (SFG) spectroscopy is intrinsically sensitive to non-centrosymmetric assemblies of molecules. Consequently, the technique has been extensively used to measure the interfacial regions of charged surfaces and aqueous solutions based on the organization of molecules as well as their vibrational resonances.[41-43] In principle, these studies can offer a wealth of chemical information such as bond strength, including hydrogen bond strength, and molecular orientation of the net assembly of water. However, vibrational SFG spectroscopy convolutes the depth dependence of the bulk and interfacial SFG signal sources, which is especially problematic in the presence of non-zero surface potentials. Specifically, the wave vector mismatch for the reflection geometries commonly used in most SFG setups is on the order of 10^2 nm^{-1}, leading to third-order (bulk allowed) contributions that add to the second-order (interface-specific) SFG response depending on the interfacial potential.[55-61]

While it has been known for a while how these second- and third-order contributions are encoded in the total detected SFG signal,[62-63] the proper lineshape analysis requires knowledge of the phase relationship between these two terms and the total interfacial potential, which has remained elusive. To overcome this problem, we now combine vibrational sum frequency, non-resonant heterodyne-detected second harmonic generation (HD-SHG), and streaming potential measurements to obtain the interface-specific response for the fused silica/water interface as a function of pH and a total ionic strength of 50 mM. Our approach enables us to elucidate the net

orientation of tight and loose hydrogen bond networks in the Stern layer over fused silica for a range of bulk solution pH conditions at a constant intermediate ionic strength of 50 mM NaCl. We identify conditions where interfacial water molecules held in a tight hydrogen bonded network flip their net orientation with pH, while observing no such flip in the diffuse layer. As such, we attribute the non-monotonic trend in the overall SFG intensity spectra with decreasing pH to changes in the water structure at the surface rather than changes in the diffuse layer structure. Finally, we compare these results to the total potential drop across the fused silica/water interface determined from HD-SHG. The changes in total surface potential with pH correlate with changes in the net orientation of the water in the Stern layer. Moreover, we find an important role of other contributions to the total interfacial potential on top of the GCS-only contributions. We thus provide new physical insights for charged solid/aqueous interfaces that hold the promise of developing our understanding of the EDL beyond mean field theories.

Results and Discussion.

Nonlinear Optics and Electrokinetics in the Electrical Double Layer. The intensity in our vibrational SFG spectra originates from water molecules located in networks that lack inversion symmetry. The centrosymmetry of bulk water is broken in the electrical double layer by four phenomena: hydrogen bonding of water molecules with the underlying surface, the ordering of water around adsorbed ions, the alignment of water permanent dipoles with the electric field emanating from charged sites at the surface, and the polarization of water molecules in said field. The first (hydrogen bonding with the surface) is expected to be largely responsible for the water

structure in the Stern layer,[57-58, 64] which we attribute to the second-order susceptibility $\chi_S^{(2)}$. The SFG intensity is then given by the following equation:

$$I_{\mathrm{SFG}} \propto \left|\chi_{\mathrm{total}}^{(2)}\right|^2 = \left|\chi_S^{(2)} + \chi_{DL}^{(2)}\right|^2 \qquad \text{eq. 1}$$

Here, I_{SFG} is the intensity of sum frequency light, and $\chi_{\mathrm{total}}^{(2)}$, $\chi_S^{(2)}$, and $\chi_{DL}^{(2)}$ are the total, Stern layer, and diffuse layer second-order susceptibilities, respectively. For our SFG measurements, $\chi_S^{(2)}$ describes the vibrations of all OH oscillators within the Stern layer and is dependent on the number and net orientation of these oscillators. The Stern layer thickness, and therefore the number of contributing water molecules, is intrinsically coupled to the ionic strength of the aqueous solution according to a recent XPS report of Stern layer compression with increasing salt concentration (~7 Å at 50 mM).[53] The region of aligned and polarized water molecules outside of the Stern layer is called the diffuse layer, which we quantify in equation 1 with the $\chi_{DL}^{(2)}$ term, according to

$$\chi_{DL}^{(2)} = \chi^{(3)} \int_{\mathrm{OHP}}^{\infty} \mathrm{E}_0(\mathrm{z}) \mathrm{e}^{\mathrm{i}\Delta \mathrm{kz}} \mathrm{dz} \qquad \text{eq.2}$$

Here, $\mathrm{E}_0(\mathrm{z}) = -\frac{d\Phi(z)}{dz}$ is the electric field emanating from the surface which is integrated from the plane marking the end of the Stern layer, the outer Helmholtz plane (z = OHP), to infinite distance from the interface ($\Phi(z = \infty) = 0$ V) to yield the absolute value and sign of the OHP electrostatic potential Φ_{OHP}. The OHP potential is often approximated as the zeta (ζ) potential that can be measured from electrokinetic measurements (Scheme 1).[27, 53, 65] At the salt concentration explored here (50 mM NaCl), the ζ potential is distinct from the potential directly at the silica surface owing to the screening effect of ions within the Stern layer, which attenuate the magnitude of the potential at the OHP relative to that at the surface (Scheme 1). Moreover, MD simulations by the Netz group

found that the interfacial flow was zero in pure water near an uncharged solid in the presence of an applied static surface field, although dipolar surface ordering of the solvent was present.[9] This suggests that the ζ potential determined from electrokinetic measurements based on flow at the shear plane is sensitive to different forces than the surface potential, which was non-zero. As we will discuss later on, using the ζ potential with the GCS model does not recapitulate the total interfacial potential, which we propose stems from the insensitivity of the ζ potential and the GCS model to the water and silica surface structure, both of which can evolve with changing pH. $\chi^{(3)}$ is the third-order susceptibility of water in the diffuse layer which is frequency dependent[66] and has been shown by experiments and MD simulations to be relatively constant up to 100 mM ionic strength.[56, 66]

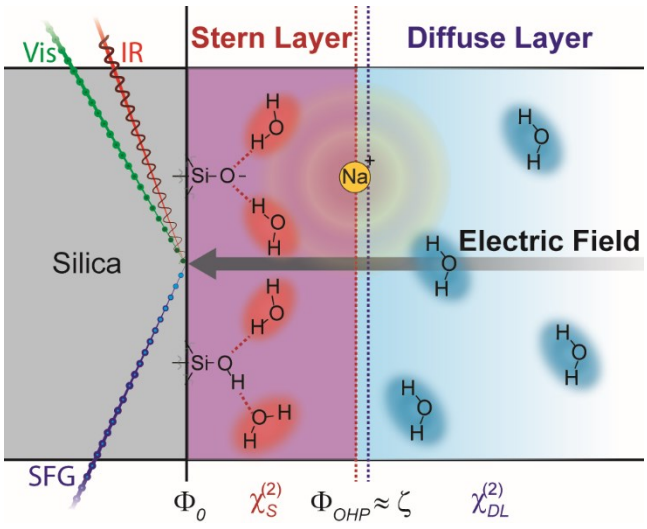

Scheme 1. The electrical double layer composed of a Stern layer (measured by $\chi_S^{(2)}$) and a diffuse layer (measured by $\chi_{DL}^{(2)}$) over negatively charged silica separated by the OHP (red dashed line). The net orientation and polarization of the diffuse layer is highlighted by the orientation of the drawn water structures, but we note a wide distribution is predicted for the diffuse layer water with its bulk-like structure.

Non-monotonic vs monotonic trends in SFG vs ζ-potential responses. Fig. 1a shows the (homodyne-detected) vibrational sum frequency generation intensity spectra of the fused

silica/water interface in the presence of 50 mM NaCl from pH 10 to 2 measured in the OH stretching region. We chose this particular ionic strength and direction in our pH titration to mimic the conditions reported in the XPS study of Stern layer thickness by Brown and co-workers.[53] Generally, three prominent features are observed that we refer to as the 3200, 3400, and 3600 cm^{-1} modes. These features arise from ordered and polarized interfacial water in the electrical double layer as described above,[43] although there is debate whether the 3600 cm^{-1} mode originates from isolated silanols[67-68] or water molecules dangling over hydrophobic silica sites.[69-70] At pH 10, the integrated SF intensity, which approximates the amount of net ordered and polarized water in the entire electrical double layer, is the largest (Fig. 1b). As the pH is lowered, the total SFG intensity decreases until pH 4 and then increases again slightly until pH 2, which lies near the point-of-zero charge (PZC) for silica, generally taken to be below pH 3, if any.[71] The origin of this non-monotonic trend, which we had observed previously at 100 mM and higher salt concentration,[72-74] is attributed to contributions to the nonlinear responses from the Stern and diffuse layers. Since these two components are convoluted in the SFG intensity measurements,[75] and further entangled with the electrostatic field across the interface, the exact origin of the non-monotonic trend is not yet clear.

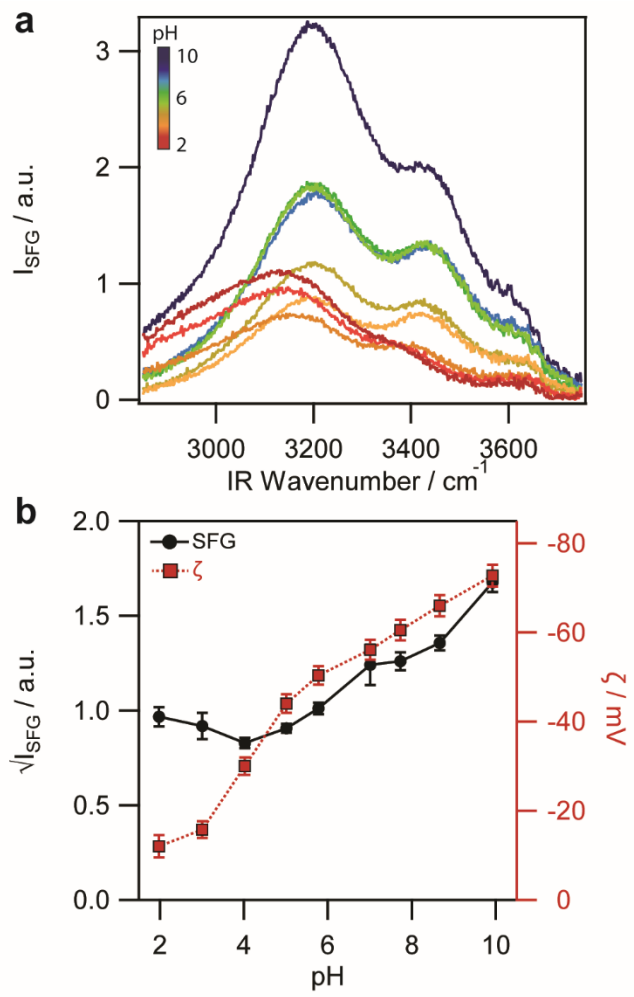

Figure 1. a) Vibrational sum frequency generation intensity spectra corrected for local field effects, (b) average square root of the integrated SFG intensities (left axis, black circles) from 2850-3750 cm^{-1}, and ζ potentials (right axis, red squares) determined by streaming potential measurements of the silica/aqueous interface in the presence of 50 mM NaCl from pH 10 to 2. SFG error bars are the standard deviation from 3 experimental replicates. ζ potential error bars are the propagated measurement errors from 2 experimental replicates.

We can, however, estimate the behaviour of the diffuse layer contribution to the SF intensity if 1) the total OHP potential is known and 2) if the $\chi^{(3)}$ spectrum for the diffuse layer waters in the silica/water interface is known for our experimental conditions. The former can be approximated by measuring the ζ potential, while the latter is known from the literature.[56, 64, 66] Fig. 1b shows that our observed ζ potentials decreased monotonically in magnitude from high to

low pH, consistent with an isoelectric point below pH 2 for this type of silica and salt concentration.[71] Therefore, the diffuse layer contribution should only decrease with decreasing pH as $\chi^{(3)}$ is invariant with pH[66] and $\chi_{DL}^{(2)}$ is thereby only modulated by the Φ_{OHP}. With this insight it is clear that the Stern layer $\chi_S^{(2)}$ is playing a large role in the non-monotonic SF intensity changes observed below pH 4.

The Stern layer contribution, $\chi_S^{(2)}$, can be obtained by subtracting the diffuse layer contribution, $\chi_{DL}^{(2)}$, from the total nonlinear susceptibility, $\chi_{total}^{(2)}$. To determine the complex $\chi_{total}^{(2)}$ spectra, we require the phase, φ, of the SFG signal where $\left|\chi_{total}^{(2)}\right|e^{i\varphi} = Re\chi_{total}^{(2)} + iIm\chi_{total}^{(2)}$, which can be estimated using the maximum entropy method.[64, 76-85] However, the maximum entropy method phase (φ_{MEM}) is not the true phase of the SFG signal, φ. The difference between the two is called the error phase ($\varphi - \varphi_{MEM}$ = error phase). Determining the error phase is the main challenge of using the maximum entropy method to predict complex spectra as it must come from some external knowledge of the system.[86] Our previous work suggested that the error phase depended on the Debye length (i.e. the ionic strength), as the Debye length describes the depth of the diffuse layer (~4 κ^{-1}) and thus determines the phase matching condition for interference between the SFG signals generated throughout the various regions within the electrical double layer and the zero plane. The resulting phase shift is not captured by the MEM phase and, accordingly, must manifest as a shift in the error phase.[64]

Phase Relation between the Stern Layer $\chi_S^{(2)}$ and the Diffuse Layer $\chi_{DL}^{(2)}$. In our present work, the salt concentration, and accordingly the Debye length, is maintained constant. Therefore we would not expect a change in error phase, as we demonstrated recently that the error phase changes systematically with Debye length owing to the dependence of the error phase on the thickness of

the diffuse layer.[64] Furthermore, at 50 mM NaCl the signal phase shift arising from optical interference in the diffuse layer should be less than 1°. Surprisingly however, we observed a significant error phase change (~70° at 3300 cm^{-1}) when we analyzed the $\left|\chi^{(2)}_{total}\right|^2$ spectra and $\chi^{(2)}_{total}$ specta from Myalitsin et al.[87] at pH 7 and pH 2 at 10 mM ionic strength using the MEM (Fig. S6). Using their[87] complex spectrum at pH 2 and our[64] complex spectrum at pH 6 as references, the error phases of our spectra herein were observed to decrease by ~100° (at 3300 cm^{-1}) from pH 6 to 2 (Fig. 2a). To understand this unexpected outcome, we turned to another nonlinear optical technique that has been used to measure phase changes at the silica/water interface, namely nonresonant heterodyne-detected second harmonic generation (HD-SHG) spectroscopy.[88-91] As we demonstrated recently, the phase shift measured by HD-SHG is related to the total sum frequency phase shift under conditions where the Debye length is changing,[64] suggesting their origins are related.

We therefore measured the SHG phase, φ_{sig}, between pH 10 and 2 at 50 mM NaCl by recording SHG intensity interferograms (Fig. 2b) from the fused silica/water interface as described in our earlier work (see SI Section S2).[88-91] Here, we report the relative phase, $\Delta\varphi_{sig}$, referenced to pH 5.8 and 50 mM NaCl and find that a phase shift in HD-SHG does indeed occur over the pH range (Fig. 2a and 2b). We highlight this phase shift is plainly visible in the HD-SHG raw interferograms evident by the shift in α-quartz positions of the maximum intensities measured at pH 10 and 2 (Fig. 2b, each mm distance corresponds to 3.158 degrees in phase). Fig. 2a also compares the relative phase change observed by HD-SHG and the change in error phase determined from our MEM analysis of the two reported complex spectra at pH 2 and 6. The HD-SHG phase shift is approximately two to three times smaller than the SF phase shift predicted at 3300 cm^{-1} using the MEM analysis. We hypothesize that this difference, which we did not observe

when changing ionic strength,[64] is attributable to the differences between resonant SFG and nonresonant SHG relative signal magnitudes and phases of contributing oscillators (i.e. the $\chi_S^{(2)}/\chi_{DL}^{(2)}$ ratio) as these should impact the resulting total phase of the signal. Moreover, the nonresonant SHG signal contains contributions from all polarizable species including interfacial silanol groups, water, the ions, and protonated and deprotonated surface sites, whereas our vibrational SFG measurements only probe OH oscillators.[61, 74, 91] Nevertheless, the HD-SHG measurements allow us to predict how the error phase changes between our two reference points (i.e. pH 6 and pH 2) (Fig. 2a, blue line).

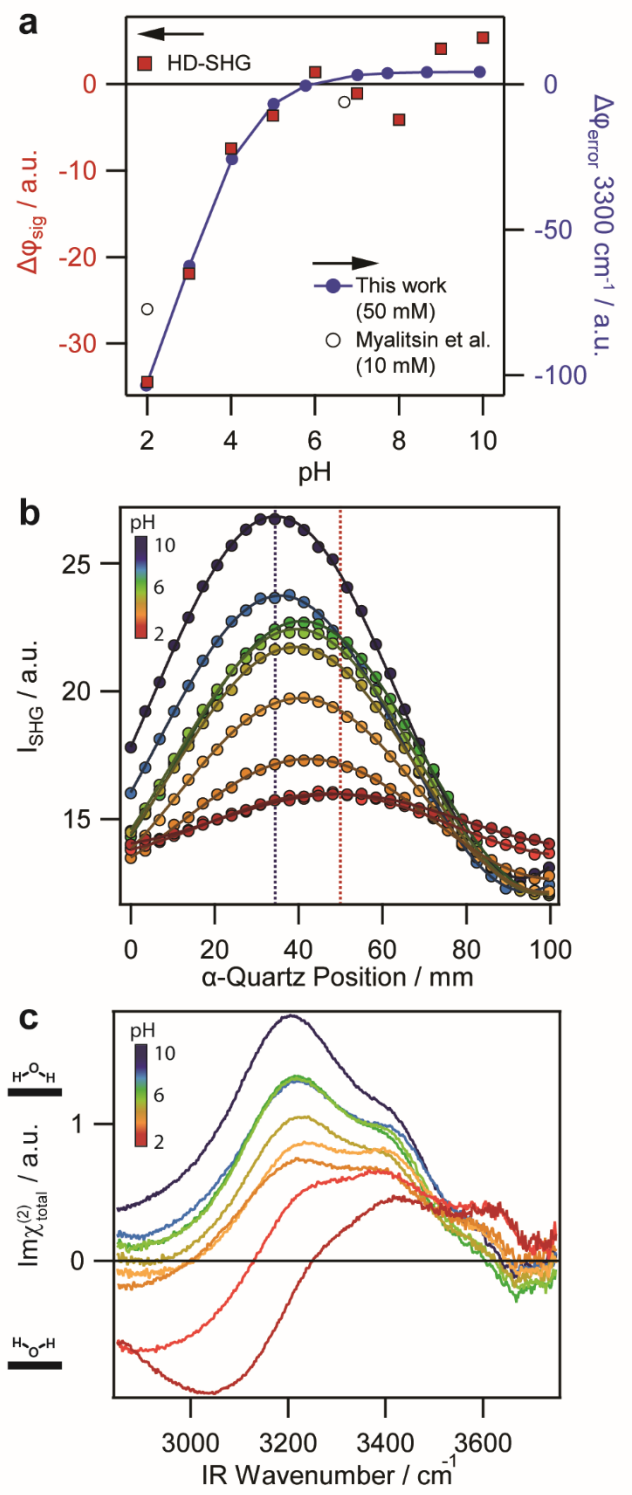

Figure 2. a) HD-SHG amplitudes and phases (red squares, left axis), and predicted error phase changes (blue line, right axis) at the silica/water interface in the presence of 50 mM NaCl from pH 10 to 2. Error phase changes determined from reported HD-SFG measurements of the silica/10 mM sodium phosphate interface are shown as open circles (right axis).[87] Changes in HD-SHG and error phases (at 3300 cm^{-1}) are relative to their values at pH 5.8. b) Representative HD-SHG

interferograms where solid lines are the cosine fits to the data (circles) and the blue and red dashed vertical lines indicate local maxima at pH 10 and 2, respectively. c) Imaginary $\chi^{(2)}_{total}$ spectra at the silica/50 mM NaCl interface determined using the maximum entropy method with reference to reported HD-SFG measurements.[64, 87]

With the error and SHG phases at each pH in hand, we performed the maximum entropy analysis of the spectra in Fig. 1a to yield $\left|\chi^{(2)}_{total}\right|e^{i\varphi_{MEM}}$ that was used to find the total complex spectra, $\left|\chi^{(2)}_{total}\right|e^{i\varphi} = Re\chi^{(2)}_{total} + iIm\chi^{(2)}_{total}$ from pH 10 to 2. The imaginary components of the spectra, $Im\chi^{(2)}_{total}$, report on the net orientation of the entire electrical double layer (Stern + diffuse layer) and are provided in Fig. 2c. At pH 10, $Im\chi^{(2)}_{total}$ is positive over the entire OH stretching region, indicating the net orientation of the water molecules that contribute in the EDL is with the hydrogen atoms pointed towards the silica.[64] As the pH is lowered, the 3200 and 3400 cm^{-1} modes decrease in magnitude while the 3600 cm^{-1} mode grows larger. Additionally, a broad negative feature around 3000 cm^{-1} appears and increases in magnitude as pH decreases. These general trends are consistent with the complex spectra measured by Myalitsin et al. at the silica/water interface and pH 2.1, 7.2, and 12.1[87] and also by Ostroverkhov et al. at the α-quartz/water interface,[92] which had been carried out over a similar pH range but at unspecified (and thus uncontrolled) ionic strengths. We emphasize that, although the work by Myalitsin et al. attempted to suppress the diffuse layer contributions through the addition of 2 M NaCl leading to a heavily modified surface water structure, neither of these prior studies reported $Im\chi^{(2)}_{S}$, i.e. they did not disentangle the Stern and diffuse layer contributions that are encoded in $\chi^{(2)}_{total}$.

The change in sign of $Im\chi^{(2)}_{total}$ with decreasing pH is attributed to a net flip in the orientation of water molecules held in a strong hydrogen-bonding network.[93-94] According to eqn. 1 and 2, $Im\chi^{(2)}_{total}$ reports predominantly on Stern layer water molecules at pH 2, where the

electrical potential is presumably small (and probably different from zero). However, at higher pH values, where the OHP potential, and hence the contribution from diffuse layer water molecules, is large, it is unclear how the Stern layer water molecules behave.

How Water Structure in the Stern and Diffuse Layer Vary with pH. To retrieve the Stern layer response, $\chi_S^{(2)}$, at all pH values, we multiply our previously determined $\chi^{(3)}$ spectrum for this interface and experimental geometry[64] by the OHP potentials we obtained from the streaming potential measurements and then subtract the resulting $\chi^{(3)} \cdot \Phi(z)$, i.e. $Im\chi_{DL}^{(2)}$, from $Im\chi_{total}^{(2)}$ as the diffuse layer lineshape is a property of bulk water and is consistent from interface to interface.[56-57, 66, 95-96] The resulting pH-dependent $Im\chi_S^{(2)}$ and $Im\chi_{DL}^{(2)}$ spectra are shown in Fig. 3a and 3b, respectively. Within the Stern layer response, $\chi_S^{(2)}$, there may be a unique surface potential-dependent term arising from Stern layer water molecules that are oriented by the electric field near the surface (i.e. $\chi_{SL}^{(3)}\Phi_0$). Such an electric field-induced reorientation of interfacial water molecules is believed to be weaker than the existing H-bond network, based on MD simulations[97] and calculations.[64] Yet, we do not know the Stern layer third-order susceptibility, $\chi_{SL}^{(3)}$, which should exhibit a different line-shape than the diffuse layer third-order susceptibility, $\chi^{(3)}$, owing to differences in hydrogen bond structure. Consequently, we do not attempt to deconvolute any surface-potential dependence from the Stern layer spectra we present and consider the total nonlinear susceptibility in the Stern layer, $\chi_S^{(2)}$, arising from all contributions. Fig. 3a shows the dominant pH dependence occurs in the low frequency region, indicating changes in pH caused changes in the orientation of water molecules located in the strongly hydrogen-bonded network in the Stern layer. This result is consistent with a purely mathematical lineshape analysis of vibrational SFG model responses at charged aqueous interfaces, which showed the highest

sensitivity in the 3200 cm^{-1} region.[63] However it is worth noting that the spectral features are broad and arise over the entire spectral range studied, indicating, just as with bulk water,[98] the hydrogen bonding network in the Stern layer is quite complex.

As mentioned earlier, the sign of $Im\chi_S^{(2)}$ reports on waters oscillators with dipoles pointing towards the silica (positively signed modes) or towards the bulk aqueous phase (negatively signed modes). At pH 10, $Im\chi_S^{(2)}$ contains a large positive feature centred around 3150 cm^{-1}, a shallow negative feature around 3400 cm^{-1}, and a narrower positive feature at 3600 cm^{-1} (Fig. 3a). As the pH is lowered the large broad positively signed mode at low wavenumber decreases in magnitude while a similarly broad negative mode grows in at slightly redshifted frequencies. Conversely, the shallow feature around 3400 cm^{-1} flips in sign as the pH is decreased. Near the point-of-zero-charge around pH 2, a large negatively signed feature around 3050 cm^{-1} is observed. Based on its sign, this mode can be assigned to water molecules that accept H-bonds from the surface while the smaller positively signed feature around 3400 cm^{-1} can be assigned to water molecules which donate H-bonds to silica.[59, 87] The similarity of the Stern layer spectrum at pH 2 to the reported silica/HOD spectrum at pH 2,[87] where no intramolecular coupling is expected, supports the claim that these broad modes arise mainly from different water populations participating in tighter (<3300 cm^{-1}) and looser (3300 cm^{-1} to 3500 cm^{-1}) hydrogen bond networks rather than intramolecular coupling. We also note that the net orientation of the water molecules in the tighter vs looser hydrogen bond network tends to be opposite from one another at any given pH, and that their pH dependence is also counter to one another.

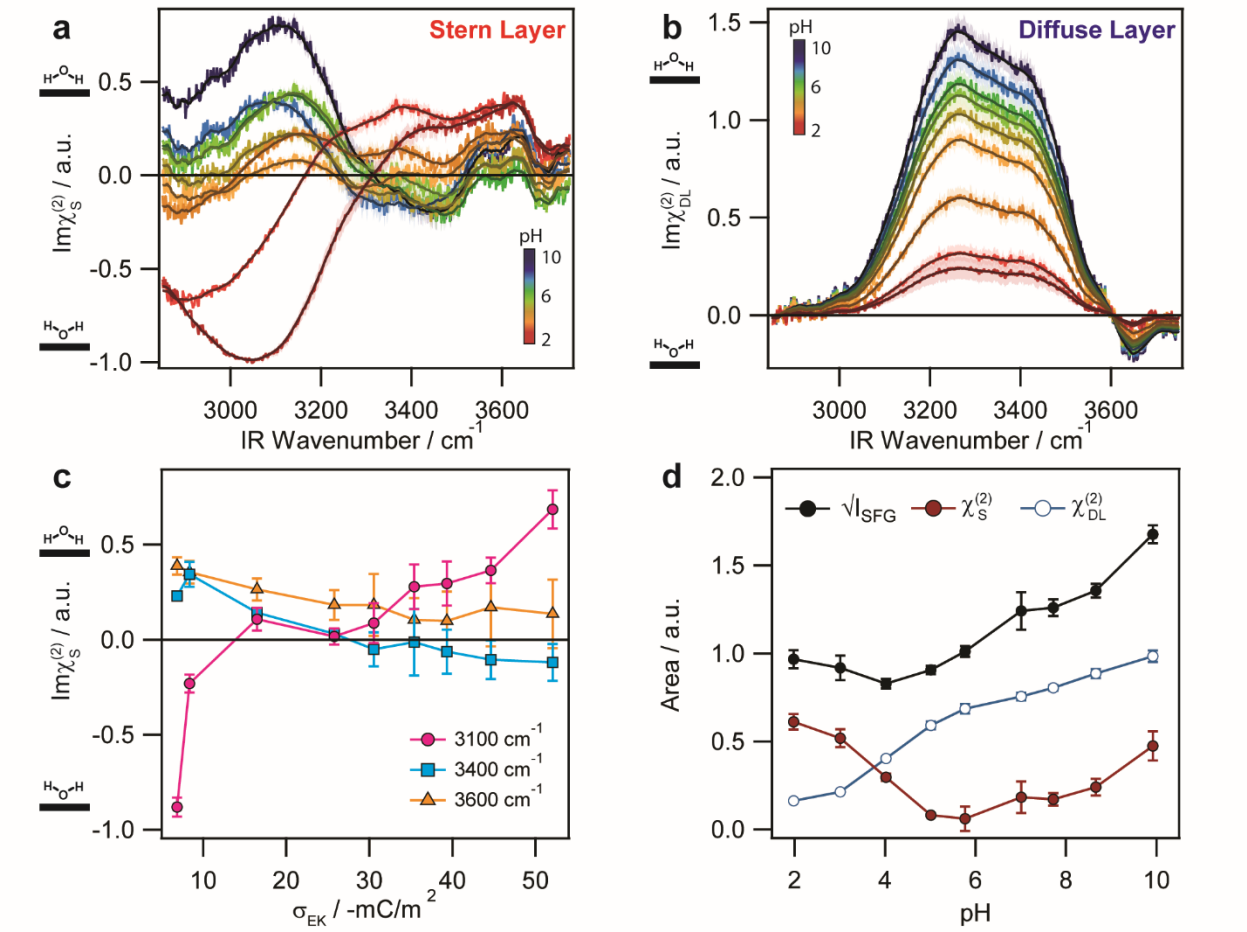

Figure 3. Contributions to the total imaginary complex spectra, $Im\chi_{total}^{(2)}$, of the silica/water interface in the presence of 50 mM NaCl from pH 10 to 2 originating from a) the Stern layer and b) the diffuse layer. Shaded areas are the propagated ζ potential and $\chi^{(3)}$ errors. Imaginary spectra have been smoothed for clarity. c) $Im\chi_S^{(2)}$ magnitudes at 3100, 3400, and 3600 cm^{-1} with respect to electrokinetic charge densities calculated from the ζ potentials. d) Average square root of the integrated SFG intensities (black squares), the Stern layer (red closed circles), and the diffuse layer (blue open circles) contributions to the total complex spectra, $\chi_{total}^{(2)}$.

Each surface silanol group can, in principle, coordinate two H-bond donor water molecules and one H-bond acceptor water, but the 3400 cm^{-1} mode attributed to the former is smaller than the 3050 cm^{-1} mode, possibly due to partial cancellation of signal contributions from some oppositely oriented H-bond donors.[59, 74] The decrease in magnitude of both the negatively signed 3050 cm^{-1} mode and the positively signed 3400 cm^{-1} mode with increasing pH is consistent with

silanol deprotonation (Fig. 3c, charge densities from our pH-dependent ζ potential measurements). Concurrently, the increase in magnitude of the positively signed mode around 3150 cm^{-1} with increasing pH is consistent with an increasing number of water molecules which donate H-bonds to siloxide sites.[64, 99] However, the steep magnitude decrease at 3100 cm^{-1} with an increase in surface charge density is noteworthy as it reveals that the number of hydrogen-bond accepting water molecules quickly reduces as the surface is deprotonated despite the substantial amount of silanol sites that should remain even at the highest pH (80% of sites at pH 10 are still neutral SiOH groups, according to XPS data).[52] Given the large number of silanol sites that are expected even at pH 10, the Stern layer $Im\chi_S^{(2)}$ spectra at high pH are surprising as they indicate that water is predominantly oriented with hydrogens towards the surface despite the large proportion of neutral silanol sites. Fig. 3c then suggests that the number of water molecules contributing to each population of the two types of hydrogen bond networks within the Stern layer is influenced not only by the number of sites but also interactions between the oriented water molecules and the electric field and charges within the Stern layer, which is in agreement with a very recent report on silica particles.[100] We speculate whether this phenomenon is primarily due to the presence of the ions within or near the Stern layer as the ion concentration within the Stern layer is intrinsically coupled to the surface charge density via the surface potential.[53] Such an ion-induced water network restructuring is supported by recent time-resolved SFG measurements[101] at low pH and our own findings at neutral pH over a wide ionic strength range.[64] Yet we caution that inferring the number density of water molecules contributing to each mode is difficult as we do not know the hyperpolarizability magnitudes or the orientation distribution of the different water populations, which adds to the complexity in interpreting these Stern layer spectra.[59, 74]

The positively signed 3600 cm^{-1} peak, which was observed in the intensity spectra and previously assigned to either isolated silanol groups[67-68] or dangling water molecules over hydrophobic sites,[69-70] is present in the Stern layer spectra and remains positively signed over the entire titration (Fig. 3c). Its pH-invariant sign is consistent with the notion that this mode originates from OH oscillators that are directed with their hydrogen pointed away from the water and into the silica. These are presumably SiOH groups located in water-inaccessible sub-nanosized pockets that are part of the $\chi^{(2)}$-active interfacial region. Our recently published AFM scans of the fused silica used in the HD-SHG experiments (Hyperion) show an rms-roughness of 0.4 nm with height variations of up to 1 nm,[91] which would be consistent with this interpretation.

The origin of the negatively signed 3400 cm^{-1} feature at high pH is unclear, however it may arise from uncoupled H-bond donor water molecules near SiO^- groups; at 2 M NaCl and pH 12, Urashima et al. determined the OH oscillators contributing to their HD-SFG spectra in this range were completely uncoupled owing to the similarity between the silica/H_2O and silica/HOD interfaces.[99] In those spectra, a small negatively signed feature around 3500 cm^{-1} was also observed, which was assigned to the uncoupled OH oscillator of the aforementioned H-bond donor water directed into the bulk water.

Our analysis reveals that the OH oscillators in the Stern layer flip their orientation as the pH changes from pH 10 to 2, except for those resonating at 3600 cm^{-1}. This trend is not apparent from the intensity spectra or even the $Im\chi^{(2)}_{total}$ spectra. Integrating the $\chi^{(2)}_S$ spectra over the entire frequency range studied (Fig. 3d) reveals the non-monotonic trend observed in the SFG intensity spectra (Fig. 1), with a minimum occurring at pH 6. The greatest amount of ordered and net-polarized water molecules in the Stern layer occurs near the PZC at pH 2. Furthermore, at pH 2 the H-bond network is apparently stronger than at higher pH, which is evident from the relatively

redshifted frequencies. In contrast, the integrated diffuse layer spectra only increase in magnitude as the pH is increased. We conclude that the non-monotonic trend observed in the SFG intensity spectra originates entirely from the water molecules located within the tight and loose hydrogen bond networks of the Stern layer.

Connecting Stern Layer Structure with Gouy-Chapman-Stern, Dipole, and Other Contributions to Φ_{tot}. Finally, we analyze the pH-dependent HD-SHG measurements from Fig. 2b to yield an interfacial potential value for each pH. In contrast to the ζ potential, this HD-SHG measurement yields the total interfacial potential drop across the solid/liquid interface and is the sum of GCS, dipolar, quadrupolar, and other contributions to the total electrostatic potential difference between the bulk silica and the aqueous bulk stemming from all species involved (not just the water molecules).[91] Our earlier pH titration at 0.5 M NaCl showed this potential to map 1:1 onto potential estimates from impedance measurements of oxide-terminated FETs.[102-103]

In the 50 mM pH titration analyzed here, the HD-SHG-determined (i.e. total surface) potential becomes neutral near pH 3 and positive at lower pH (+31 ± 20 mV at pH 2, Fig. 4).[91] In contrast, our streaming potential measurements (Fig. 1b) indicate that the ζ potential remains negative over the entire pH range (pH 10 to pH 2, 50 mM ionic strength, Fig. 1b). Oppositely signed surface potentials (measured by an ion-sensitive FET device, which also provides the total surface potential) and ζ potentials have also been observed near the point-of-zero-charge of a single crystal quartz electrode in 10 mM NaCl.[32] We provide two explanations for the opposite signs between the ζ potentials (arising at the outer Helmholtz plane) and the total interfacial potential Φ_{total} (arising at the 0-plane). The first explanation stems from the observed flip in net orientation of the tightly H-bonded water molecules in the Stern layer (contributing at 3100 cm^{-1}) at ~ pH 4 as the pH decreases from pH 10 to 2 (Fig. 3a). It has been argued that like in FET- and

X-ray- based measurements of the surface potential, the total potential that is probed by HD-SHG includes not only the Gouy-Chapman contribution but all dipole and higher order contributions from the ordered water molecules and the silica surface.[91] As mentioned earlier, electrokinetic measurements of the ζ potential appear to be insensitive to the ordering of water based on the simulations of Netz and co-workers where no ζ potential (no flow) was observed at an uncharged surface despite the presence of an applied static field and the ordering of the surface water molecules.[9] In contrast, water dipoles have been known to play a key role in the electrical and structural properties of the EDL over electrochemical interfaces in the form of the "δχ potential" (no relation to $\chi^{(2)}$ or $\chi^{(3)}$).[23, 104] Moreover, simulations have found that contributions from higher-order moments were also important in determining the surface potential at liquid/vapor water interfaces.[22]

As shown in Fig 4, we observe a connection between the integrated $Im\chi_S^{(2)}$ (surface) spectra, which report on the order and net direction of the water molecules in the Stern layer, and the total interfacial potential measured by HD-SHG. At pH 10, the Stern layer is highly ordered with the net orientation of water molecules pointing their hydrogen atoms towards the surface leading to a positive value from the integrated $Im\chi_S^{(2)}$. At this pH, the total potential from the HD-SHG analysis is substantially more negative than the ζ potential at pH 10, consistent with the former containing contributions to the potential beyond those predicted from the Gouy-Chapman Stern model (-330 mV vs -73 mV).[91] Using a Gouy-Chapman-Stern model to calculate the surface potential (Φ_0), which was -210 mV at pH 10 (see supporting information for details), the remaining contribution to the total interfacial potential is ~ -120 mV at pH 10. This significant value is consistent with the large dipole potentials on the order of hundreds of millivolts measured at the neat water/air interface using ionizing surface potential methods.[11] As the pH is lowered, this

remaining potential value inverts sign from negative to positive, which mirrors the flip in orientation observed in the imaginary Stern layer spectra (Fig. 4). At pH 2, the remaining potential is approximately +43 mV, and the Stern layer is well ordered with the water molecules net-oriented with their oxygen atoms now pointed towards the surface (negative features in $Im\chi_S^{(2)}$). The GCS contribution to the total interfacial potential in Fig 4 assumes that the surface charge is still slightly negative at pH 2 (i.e. more SiO^- than positive sites). Based on this scenario, the HD-SHG-determined potential could be positive at pH 2 because the significant contribution from the water in the Stern layer overwhelms the oppositely charged surface Gouy-Chapman potential (Fig. 4), while the ζ potential at the outer Helmholtz plane is still negative.

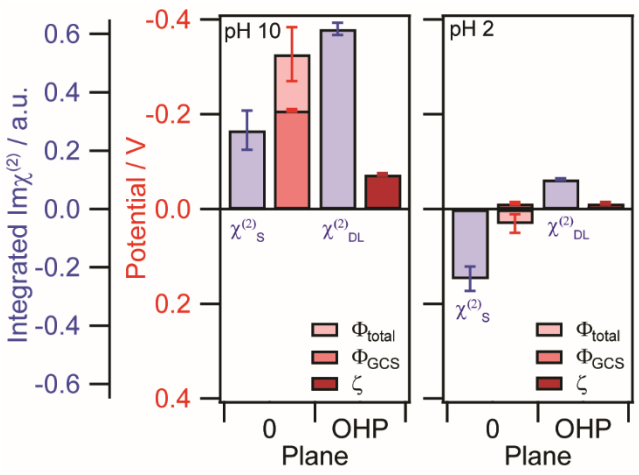

Figure 4. Interfacial potentials at the silica/50 mM NaCl interface at surface (0) and outer-Helmholtz (OHP) planes at pH 10 and 2. The Gouy-Chapman-Stern contribution at the 0-plane was calculated using surface charge densities determined from a silica deprotonation model.[96, 105] At pH 10, a large contribution to the total interfacial potential is unaccounted for. At pH 2, Φ_{GCS} is opposite in sign to Φ_{total} either due to charge overcompensation or an unknown contribution to the total potential from the waters and silica. The net water alignment in the Stern and diffuse layers is estimated from the $Im\chi^{(2)}$ spectra integrated from 2850-3750 cm^{-1}. The aligned water in the Stern layer tracks the total potential sign inversion at the 0-plane.

The second scenario is a simpler explanation, but not mutually exclusive from the first, for the different signed potentials from SHG and streaming potential measurements at pH 2, which is expected to be near and even below the pzc.[71] If the silica surface (0-plane) is actually net

positively charged at pH 2 as a result of a greater number of positive protonated sites compared with negative deprotonated ones,[52] then the Stern layer at pH 2 would exhibit a static electric field directed away from the surface, aligning Stern layer waters with their hydrogens pointed away from the surface. Additionally, the presence of a heavily protonated surface would align waters in the same direction due to the preferential hydrogen bonding with water acting as hydrogen acceptor. This net orientation of the Stern layer waters are consistent with the sign of the large low wavenumber mode in the Stern layer spectra at low pH (Fig. 3a). Then how to account for the negative ζ potential? One possibility is charge reversal where the amount of ions near the surface (in the Stern layer) overcompensates the amount of charge on the surface.[106] This phenomenon has been observed for a variety of surfaces and attributed to both physical (eg. ion-ion correlations) and chemical (eg. ion-surface complexation) mechanisms.[107] For positively charged silica, the chloride would be expected to be concentrated at the surface; but charge reversal would require the concentration near the surface to exceed the positive charges. However, overcompensation by monovalent ions is less known than multivalent ions.[106-108] Nevertheless, MD-DFT calculations at the neutral quartz/aqueous interface did observe chloride interacting closely with the neutral surface albeit while maintaining the chloride hydration shell.[109] Future work will explore the impact of different counter-ions particularly near the point-of-zero charge to help distinguish between the two proposed mechanisms.

We note, however, that it is not straightforward to relate the net direction of the water in the Stern layer with the sign of the remaining potential. For example, the internal electric field arising from the dipole moments of water, which clearly opposes the surface field at pH 10, is also opposite to the field generated immediately outside the dipole of water making it less intuitive to relate the net orientation of water and the resulting dipole potential. Moreover, simulations of the

liquid-vapor water interface revealed that the net dipole potential and quadrupole potential of water were oriented in opposite directions.[22] For our system, the relative importance of the dipole and the higher order moments to the total potential is unknown. Nevertheless, our experimental results are consistent with a physical picture that is more complex than what mean field (Bragg-Williams) type approaches would predict.[17] While dipole-only contributions may not suffice to account for all the non-GCS contributions, the correlation between the pH-dependence of the Φ_{total} and the changes in $Im\chi_S^{(2)}$ suggest we capture the dependence of Φ_{total} on the water structure in the Stern layer (Fig. 4).

New questions and problems that we can now address include the following: as the interfacial acid base chemistry of silica only involves around 10 to 15% of surface sites,[52] could there be an outsized influence of a minority population of Stern layer water molecules on the SFG lineshapes? Are the magnitudes of the orientationally averaged molecular hyperpolarizabilities of the Stern layer water molecules in the tight (3200 cm^{-1}) and more loose (3400 cm^{-1}) H-bonding networks the same or different[74]? How many SFG-active water molecules are comprised in each of these two broad classes of H-bonding environments? While these problems are currently underdetermined from an experimental perspective, our new insights into the kinds of SFG lineshapes that Stern layer water molecules produce provide a direct link to experimentally validate atomistic computer simulations of interfacial water structures and their second-order nonlinear susceptibilities. We thus envision joint experimental-computational investigations of charged aqueous interfaces to address these new science questions.

Conclusions

In summary, we separated the vibrational sum frequency signal from the silica/water interface into Stern and diffuse layer contributions using the maximum entropy method,

complementary heterodyne-detected second harmonic generation, and streaming potential measurements while appropriately accounting for phase matching and absorptive-dispersive mixing. The integrated SFG intensities reporting on the total amount of ordered water in the EDL exhibited a non-monotonic trend with a minimum at pH 4. Yet, ζ potential measurements at the same interface only decreased in magnitude with decreasing pH. Since the ζ potentials are responsible for aligning the diffuse layer water molecules, the non-monotonic trend observed by SFG was identified to originate from Stern layer water molecules in tight and loosely H-bonded networks. The maximum entropy method was used with error phases determined from previous phase-sensitive SFG[64, 87] and complementary heterodyne-detected SHG experiments to retrieve the complex SFG spectra from the measured intensities, for which the imaginary component reports on the net absolute molecular orientation of the EDL water structure. The Stern layer spectra, $\chi_S^{(2)}$, were then obtained by coupling our recently determined $\chi^{(3)}$ spectrum[64] to the measured ζ potentials and subtracting the resulting diffuse layer spectra, $\chi_{DL}^{(2)}$, from the total complex spectra, $\chi_{total}^{(2)}$, derived from the maximum entropy method.

The imaginary parts of the Stern layer spectra exhibited a flip in sign upon decreasing the pH from 10 to pH 2, particularly for water molecules in the tight H-bond network (stretching frequencies <3300 cm^{-1}). The minimum structural order occurred at pH 6 at this salt concentration of 50 mM, while the maximum structural order occurred at pH 2 and pH 10. The change in $Im\chi_S^{(2)}$ with respect to pH did not linearly follow the charge density calculated from the ζ potentials. Furthermore, the lineshape changes were larger than would be expected for a surface that maintains ~80% SiOH sites throughout the entire pH range studied.[52] These results hint at further complexity to the behaviour of the Stern layer waters in relation to charge density.

We found from the total potential drop across the fused silica/electrolyte interface provided by our HD-SHG experiments that the Gouy-Chapman-Stern-only contribution vastly underestimates the total interfacial potential. Indeed, over one-third of the total potential at pH 10 and 2 is due to non-GCS contributions, presumably from dipolar, quadrupolar, and higher order contributions from solvent and other species that are not captured in the pH-independent relative permittivity constant used in the GCS models. We also suggest that these contributions are not sampled in electrokinetic measurements, such as streaming potentials, based on MD simulations by Netz and co-workers,[9] and we provide an estimate of the difference in the GCS surface potential and the total potential for the various pH values investigated. Additionally, we found the flip in net orientation of the Stern layer waters mimics the flip in sign of this total surface potential, suggesting they are related.

Our findings underscore the importance of properly accounting for the $\chi^{(3)}$ contribution in the analysis of the vibrational lineshapes provided by second-order spectroscopic studies of charged aqueous interfaces. The method presented here, in which SFG and SHG spectroscopy are paired, is proposed as a clear path to take. Taken together, our results provide the first vibrational Stern layer spectra of the silica/water interface over a wide pH range at controlled ionic strength. Moreover, they indicate an important role of non-GCS contributions to the total potential drop across the oxide/water interface, accounting for greater than half and more, depending on pH. Our analysis may be applied to many charged surface/aqueous interfaces to spectrally separate the Stern and diffuse layers given the appropriate complex spectra are available for reference.

ASSOCIATED CONTENT

Supporting Information

The following files are available free of charge via the Internet at https://pubs.acs.org.

The supporting information contains: experimental details, streaming potential experimental replicates, comparison of HD-SHG potentials from different silica suppliers, electrokinetic charge densities calculated from ζ potentials, a Gouy-Chapman-Stern model, calculations for local field effects in SFG spectra, in-depth details of error phase prediction using the MEM, and a sensitivity analysis for the error phase at pH 2.

AUTHOR INFORMATION

Corresponding Author

*E-mail: julianne.gibbs@ualberta.ca (J.M.G.)

*E-mail: f-geiger@northwestern.edu (F.M.G.)

Notes

The authors declare no competing financial interest.

ACKNOWLEDGEMENTS

J.M.G. gratefully acknowledges the Natural Sciences and Engineering Research Council of Canada for an Accelerator Award, the Alfred P. Sloan Foundation for a Research Fellowship, and Petro-Canada for a Young Innovator Award. B.R. gratefully acknowledges support from the Alberta/Technical University of Munich International Graduate School for Hybrid Functional Materials (ATUMS-NSERC CREATE) program, the Natural Sciences and Engineering Research Council of Canada for a Canadian Graduate Scholarship, and the Queen Elizabeth II Graduate Scholarship. F.M.G. and E.M. gratefully acknowledge support from the AFOSR Molecular Dynamics and Theoretical Chemistry Program and from Northwestern University. We thank Dr. Dennis K. Hore (University of Victoria), Dr. Christopher Mundy (Pacific Northwest National Laboratory), and Dr. Eric Tyrode (KTH Royal Institute of Technology) for insightful discussions.

REFERENCES

1. Langmuir, D., *Aqueous Environmental Chemistry*. Prentice Hall: Upper Saddle River, NJ 1997.
2. Lyklema, J., *Fundamentals of Interface and Colloid Science*. Elsevier: 2000.
3. Helmholtz, H., Ueber Einige Gesetze der Vertheilung Elektrischer Ströme in Körperlichen Leitern mit Anwendung auf die Thierisch-Elektrischen Versuche. *Ann. Phys.-Berlin* **1853,** *165* (6), 211-233.
4. Gouy, M., Sur la Constitution de la Charge Électrique à la Surface d'un Électrolyte. *J. Phys. Theor. Appl.* **1910,** *9* (1), 457-468.
5. Chapman, D. L., LI. A Contribution to the Theory of Electrocapillarity. *Philos. Mag.* **1913,** *25* (148), 475-481.
6. Stern, O., Zur Theorie der Elektrolytischen Doppelschicht. *Z. Elktrochem. Angew. P.* **1924,** *30* (21-22), 508-516.
7. Grahame, D. C., The Electrical Double Layer and the Theory of Electrocapillarity. *Chem. Rev.* **1947,** *41* (3), 441-501.
8. Casper, C. B.; Verreault, D.; Adams, E. M.; Hua, W.; Allen, H. C., Surface Potential of DPPC Monolayers on Concentrated Aqueous Salt Solutions. *J. Phys. Chem. B* **2016,** *120* (8), 2043-2052.
9. Bonthuis, D. J.; Horinek, D.; Bocquet, L.; Netz, R. R., Electrohydraulic Power Conversion in Planar Nanochannels. *Phys. Rev. Lett.* **2009,** *103* (14), 144503.
10. Rodriguez, D.; Marquez, M. D.; Zenasni, O.; Han, L. T.; Baldelli, S.; Lee, R. T., Surface Dipoles Induce Uniform Orientation in Contacting Polar Liquids. *Chem. Mat.* **2020,** *32*, 7832-41.
11. Adel, T.; Velez-Alvarez, J.; Co, A. C.; Allen, H. C., Circuit Analysis of Ionizing Surface Potential Measurements of Electrolyte Solutions. *J. Electrochem. Soc.* **2021,** *168* (1), 016507.
12. Doyle, C. C.; Shi, Y.; Beck, T. L., The Importance of the Water Molecular Quadrupole for Estimating Interfacial Potential Shifts Acting on Ions Near the Liquid−Vapor Interface. *J. Phys. Chem. B* **2019,** *123*, 3348-58.
13. Cendagorta, J. R.; Ichiye, T., The Surface Potential of the Water-Vapor Interface from Classical Simulations. *J. Phys. Chem. B* **2015,** *119*, 9114-9122.
14. Leung, K., Surface Potential at the Air-Water Interface Computed Using Density Functional Theory. *J. Phys. Chem. Lett.* **2010,** *1*, 496-9.
15. Ma, E.; Kim, J.; Chang, H.; Ohno, P. E.; Jodts, R. J.; Miller III, T. F.; Geiger, F. M., Stern and Diffuse Layer Interactions during Ionic Strength Cycling. *J. Phys. Chem. C* **2021,** *125*, 18002-14.
16. Chen, S.-H.; Singer, S., Molecular Dynamics Study of the Electric Double Layer and Nonlinear Spectroscopy at the Amorphous Silica- Water Interface. *J. Phys. Chem. A* **2019,** *123*, 6364-84.
17. Dewan, S.; Carnevale, V.; Bankura, A.; Eftekhari-Bafrooei, A.; Fiorin, G.; Klein, M. L.; Borguet, E., Structure of Water at Charged Interfaces: A Molecular Dynamics Study. *Langmuir* **2014,** *30*, 8056-65.
18. Becker, M. R.; Loche, P.; Netz, R. R., Electrokinetic, Electrochemical and Electronic Surface Potentials of the Pristine Water Liquid-Vapor Interface. *Refubium FU* **2022**, http://dx.doi.org/10.17169/refubium-34416.
19. Duignan, T. T.; Mundy, C. J.; Schenter, G. K.; Zhao, X. S., Method for Accurately Predicting Solvation Structure. *J. Chem. Theory Comput.* **2020,** *16* (8), 5401-5409.
20. Duignan, T. T.; Schenter, G. K.; Fulton, J. L.; Huthwelker, T.; Balasubramanian, M.; Galib, M.; Baer, M. D.; Wilhelm, J.; Hutter, J.; Del Ben, M.; Zhao, X. S.; Mundy, C. J., Quantifying the Hydration Structure of Sodium and Potassium Ions: Taking Additional Steps on Jacob's Ladder. *Phys. Chem. Chem. Phys.* **2020,** *22* (19), 10641-10652.
21. Kathmann, S. M.; Kuo, I. F. W.; Mundy, C. J.; Schenter, G. K., Understanding the Surface Potential of Water. *J. Phys. Chem. B* **2011,** *115* (15), 4369-4377.
22. Wilson, M. A.; Pohorille, A.; Pratt, L. R., Comment on ''Study on The Liquid–Vapor Interface of Water. I. Simulation Results of Thermodynamic Properties and Orientational Structure''. *J. Chem. Phys.* **1989,** *90* (9), 5211-5213.

23. Habib, M. A., Solvent Dipoles at the Electrode-Solution Interface. In *Modern Aspects of Electrochemistry: No. 12*, Bockris, J. O. M.; Conway, B. E., Eds. Springer US: Boston, MA, 1977; pp 131-182.
24. Boamah, M. D.; Ohno, P. E.; Geiger, F. M.; Eisenthal, K. B., Relative Permittivity in the Electrical Double Layer from Nonlinear Optics. *J. Chem. Phys.* **2018,** *148* (22), 222808.
25. Fumagalli, L.; Esfandiar, A.; Fabregas, R.; Hu, S.; Ares, P.; Janardanan, A.; Yang, Q.; Radha, B.; Taniguchi, T.; Watanabe, K.; Gomila, G.; Novoselov, K. S.; Geim, A. K., Anomalously Low Dielectric Constant of Confined Water. *Science* **2018,** *360* (6395), 1339-1342.
26. Sverjensky, D. A., Prediction of Surface Charge on Oxides in Salt Solutions: Revisions for 1:1 (M+L−) Electrolytes. *Geochim. Cosmochim. Ac.* **2005,** *69* (2), 225-257.
27. Brown, M. A.; Abbas, Z.; Kleibert, A.; Green, R. G.; Goel, A.; May, S.; Squires, T. M., Determination of Surface Potential and Electrical Double-Layer Structure at the Aqueous Electrolyte-Nanoparticle Interface. *Phys. Rev. X* **2016,** *6* (1), 011007.
28. Mayordomo, N.; Foerstendorf, H.; Lützenkirchen, J.; Heim, K.; Weiss, S.; Alonso, U.; Missana, T.; Schmeide, K.; Jordan, N., Selenium(IV) Sorption Onto γ-Al2O3: A Consistent Description of the Surface Speciation by Spectroscopy and Thermodynamic Modeling. *Environ. Sci. Technol.* **2018,** *52* (2), 581-588.
29. Öhman, L. O.; Lövgren, L.; Hedlund, T.; Sjöberg, S., Chapter 1 - The Ionic Strength Dependency of Mineral Solubility and Chemical Speciation in Solution. In *Interface Science and Technology*, Lützenkirchen, J., Ed. Elsevier: 2006; Vol. 11, pp 1-34.
30. Kosmulski, M., Co-Adsorption of Mono- and Multivalent Ions on Silica and Alumina. *Ber. Bunsenges. Phys. Chem* **1994,** *98* (8), 1062-1067.
31. Fung, C. D.; Cheung, P. W.; Ko, W. H., A Generalized Theory of an Electrolyte-Insulator-Semiconductor Field-Effect Transistor. *IEEE T. Electron. Dev.* **1986,** *33* (1), 8-18.
32. Preočanin, T.; Namjesnik, D.; Brown, M. A.; Lützenkirchen, J., The Relationship Between Inner Surface Potential and Electrokinetic Potential from an Experimental and Theoretical Point of View. *Environ. Chem.* **2017,** *14* (5), 295-309.
33. Raji, F.; Ejtemaei, M.; Nguyen, A. V., Resolving the Mystery of the Second Charge Reversal on Solid Surfaces in the Presence of Divalent Heavy Metal Ions. *Appl. Surf. Sci.* **2020,** *529*, 147128.
34. de Lint, W. B. S.; Benes, N. E.; Lyklema, J.; Bouwmeester, H. J. M.; van der Linde, A. J.; Wessling, M., Ion Adsorption Parameters Determined from Zeta Potential and Titration Data for a γ-Alumina Nanofiltration Membrane. *Langmuir* **2003,** *19* (14), 5861-5868.
35. Zhang, Z.; Fenter, P.; Cheng, L.; Sturchio, N. C.; Bedzyk, M. J.; Předota, M.; Bandura, A.; Kubicki, J. D.; Lvov, S. N.; Cummings, P. T.; Chialvo, A. A.; Ridley, M. K.; Bénézeth, P.; Anovitz, L.; Palmer, D. A.; Machesky, M. L.; Wesolowski, D. J., Ion Adsorption at the Rutile−Water Interface: Linking Molecular and Macroscopic Properties. *Langmuir* **2004,** *20* (12), 4954-4969.
36. Sverjensky, D. A., Prediction of the Speciation of Alkaline Earths Adsorbed on Mineral Surfaces in Salt Solutions. *Geochim. Cosmochim. Ac.* **2006,** *70* (10), 2427-2453.
37. Morag, J.; Dishon, M.; Sivan, U., The Governing Role of Surface Hydration in Ion Specific Adsorption to Silica: An AFM-Based Account of the Hofmeister Universality and Its Reversal. *Langmuir* **2013,** *29* (21), 6317-6322.
38. van Lin, S. R.; Grotz, K. K.; Siretanu, I.; Schwierz, N.; Mugele, F., Ion-Specific and pH-Dependent Hydration of Mica–Electrolyte Interfaces. *Langmuir* **2019,** *35* (17), 5737-5745.
39. Brown Gordon, E., How Minerals React with Water. *Science* **2001,** *294* (5540), 67-69.
40. Lee, S. S.; Fenter, P.; Nagy, K. L.; Sturchio, N. C., Real-Time Observation of Cation Exchange Kinetics and Dynamics at the Muscovite-Water Interface. *Nat. Commun.* **2017,** *8* (1), 15826.
41. Geiger, F. M., Second Harmonic Generation, Sum Frequency Generation, and $\chi^{(3)}$: Dissecting Environmental Interfaces with a Nonlinear Optical Swiss Army Knife. *Annu. Rev. Phys. Chem.* **2009,** *60*, 61-83.

42. Covert, P. A.; Hore, D. K., Geochemical Insight from Nonlinear Optical Studies of Mineral–Water Interfaces. *Annu. Rev. Phys. Chem.* **2016,** *67* (1), 233-257.
43. Backus, E. H. G.; Schaefer, J.; Bonn, M., Probing the Mineral–Water Interface with Nonlinear Optical Spectroscopy. *Angew. Chem. Int. Ed.* **2021,** *60* (19), 10482-10501.
44. Nakouzi, E.; Stack, A. G.; Kerisit, S.; Legg, B. A.; Mundy, C. J.; Schenter, G. K.; Chun, J.; De Yoreo, J. J., Moving beyond the Solvent-Tip Approximation to Determine Site-Specific Variations of Interfacial Water Structure through 3D Force Microscopy. *J. Phys. Chem. C* **2021,** *125* (2), 1282-1291.
45. Harmon, K. J.; Chen, Y.; Bylaska, E. J.; Catalano, J. G.; Bedzyk, M. J.; Weare, J. H.; Fenter, P., Insights on the Alumina–Water Interface Structure by Direct Comparison of Density Functional Simulations with X-ray Reflectivity. *J. Phys. Chem. C* **2018,** *122* (47), 26934-26944.
46. Lee, S. S.; Schmidt, M.; Laanait, N.; Sturchio, N. C.; Fenter, P., Investigation of Structure, Adsorption Free Energy, and Overcharging Behavior of Trivalent Yttrium Adsorbed at the Muscovite (001)–Water Interface. *J. Phys. Chem. C* **2013,** *117* (45), 23738-23749.
47. Lee, S. S.; Park, C.; Sturchio, N. C.; Fenter, P., Nonclassical Behavior in Competitive Ion Adsorption at a Charged Solid–Water Interface. *J. Phys. Chem. Lett.* **2020,** *11* (10), 4029-4035.
48. Fenter, P.; Sturchio, N. C., Mineral–Water Interfacial Structures Revealed by Synchrotron X-Ray Scattering. *Prog. Surf. Sci.* **2004,** *77* (5), 171-258.
49. Park, C.; Fenter, P. A.; Nagy, K. L.; Sturchio, N. C., Hydration and Distribution of Ions at the Mica-Water Interface. *Phys. Rev. Lett.* **2006,** *97* (1), 016101.
50. Fenter, P.; Cheng, L.; Rihs, S.; Machesky, M.; Bedzyk, M. J.; Sturchio, N. C., Electrical Double-Layer Structure at the Rutile–Water Interface as Observed in Situ with Small-Period X-Ray Standing Waves. *J. Colloid Interf. Sci.* **2000,** *225* (1), 154-165.
51. Schlegel, M. L.; Nagy, K. L.; Fenter, P.; Sturchio, N. C., Structures of Quartz (100)- and (101)-Water Interfaces Determined by X-Ray Reflectivity and Atomic Force Microscopy of Natural Growth Surfaces. *Geochim. Cosmochim. Ac.* **2002,** *66* (17), 3037-3054.
52. Duval, Y.; Mielczarski, J. A.; Pokrovsky, O. S.; Mielczarski, E.; Ehrhardt, J. J., Evidence of the Existence of Three Types of Species at the Quartz−Aqueous Solution Interface at pH 0−10: XPS Surface Group Quantification and Surface Complexation Modeling. *J. Phys. Chem. B* **2002,** *106* (11), 2937-2945.
53. Brown, M. A.; Goel, A.; Abbas, Z., Effect of Electrolyte Concentration on the Stern Layer Thickness at a Charged Interface. *Angew. Chem. Int. Ed.* **2016,** *55*, 3790 - 3794.
54. Shi, B.; Agnihotri, M. V.; Chen, S.-H.; Black, R.; Singer, S. J., Polarization Charge: Theory and Applications to Aqueous Interfaces. *J. Chem. Phys.* **2016,** *144* (16), 164702.
55. Joutsuka, T.; Hirano, T.; Sprik, M.; Morita, A., Effects of Third-Order Susceptibility in Sum Frequency Generation Spectra: A Molecular Dynamics Study in Liquid Water. *Phys. Chem. Chem. Phys.* **2018,** *20* (5), 3040-3053.
56. Joutsuka, T.; Morita, A., Electrolyte and Temperature Effects on Third-Order Susceptibility in Sum-Frequency Generation Spectroscopy of Aqueous Salt Solutions. *J. Phys. Chem. C* **2018,** *122* (21), 11407-11413.
57. Pezzotti, S.; Galimberti, D. R.; Shen, Y. R.; Gaigeot, M.-P., Structural Definition of the BIL and DL: A New Universal methodology to Rationalize Non-Linear $\chi^{(2)}(\omega)$ SFG Signals at Charged Interfaces, Including $\chi^{(3)}(\omega)$ Contributions. *Phys. Chem. Chem. Phys.* **2018,** *20* (7), 5190-5199.
58. Pezzotti, S.; Galimberti, D. R.; Gaigeot, M.-P., Deconvolution of BIL-SFG and DL-SFG Spectroscopic Signals Reveals Order/Disorder of Water at the Elusive Aqueous Silica Interface. *Phys. Chem. Chem. Phys.* **2019,** *21* (40), 22188-22202.
59. Roy, S.; Hore, D. K., Simulated Structure and Nonlinear Vibrational Spectra of Water Next to Hydrophobic and Hydrophilic Solid Surfaces. *J. Phys. Chem. C* **2012,** *116* (43), 22867-22877.

60. Gonella, G.; Lütgebaucks, C.; de Beer, A. G. F.; Roke, S., Second Harmonic and Sum-Frequency Generation from Aqueous Interfaces Is Modulated by Interference. *J. Phys. Chem. C* **2016,** *120* (17), 9165-9173.
61. Wang, H.; Hu, X.-H.; Wang, H.-F., Charge-Induced χ(3) Susceptibility in Interfacial Nonlinear Optical Spectroscopy Beyond the Bulk Aqueous Contributions: The Case for Silica/Water Interface. *J. Phys. Chem. C* **2021,** *125* (47), 26208-26215.
62. Ohno, P. E.; Wang, H.-f.; Geiger, F. M., Second-Order Spectral Lineshapes from Charged Interfaces. *Nat. Commun.* **2017,** *8* (1), 1032.
63. Ohno, P. E.; Wang, H.-f.; Paesani, F.; Skinner, J. L.; Geiger, F. M., Second-Order Vibrational Lineshapes from the Air/Water Interface. *J. Phys. Chem. A* **2018,** *122* (18), 4457-4464.
64. Rehl, B.; Gibbs, J. M., Role of Ions on the Surface-Bound Water Structure at the Silica/Water Interface: Identifying the Spectral Signature of Stability. *J. Phys. Chem. Lett.* **2021,** *12* (11), 2854-2864.
65. Lyklema, J., *Solid-Liquid Interfaces*. Academic Press: San Diego, 1995; Vol. II.
66. Wen, Y.-C.; Zha, S.; Liu, X.; Yang, S.; Guo, P.; Shi, G.; Fang, H.; Shen, Y. R.; Tian, C., Unveiling Microscopic Structures of Charged Water Interfaces by Surface-Specific Vibrational Spectroscopy. *Phys. Rev. Lett.* **2016,** *116* (1), 016101.
67. Dalstein, L.; Potapova, E.; Tyrode, E., The Elusive Silica/Water Interface: Isolated Silanols Under Water as Revealed by Vibrational Sum Frequency Spectroscopy. *Phys. Chem. Chem. Phys.* **2017,** *19*, 10343-10349.
68. Rashwan, M.; Rehl, B.; Sthoer, A.; Darlington, A. M.; Azam, M. S.; Zeng, H.; Liu, Q.; Tyrode, E.; Gibbs, J. M., Structure of the Silica/Divalent Electrolyte Interface: Molecular Insight into Charge Inversion with Increasing pH. *J. Phys. Chem. C* **2020,** *124* (49), 26973-26981.
69. Cyran, J. D.; Donovan, M. A.; Vollmer, D.; Siro Brigiano, F.; Pezzotti, S.; Galimberti, D. R.; Gaigeot, M.-P.; Bonn, M.; Backus, E. H. G., Molecular Hydrophobicity at a Macroscopically Hydrophilic Surface. *P. Natl. Acad. Sci. USA* **2019,** *116* (5), 1520.
70. Urashima, S.-h.; Uchida, T.; Yui, H., A Hydrogen-Bonding Structure in Self-Formed Nanodroplets of Water Adsorbed on Amorphous Silica Revealed via Surface-Selective Vibrational Spectroscopy. *Phys. Chem. Chem. Phys.* **2020,** *22* (46), 27031-27036.
71. Kosmulski, M., The pH Dependent Surface Charging and Points pf Zero Charge. IX. Update. *Adv. Colloid Interface Sci.* **2021,** *296*, 102519.
72. DeWalt-Kerian, E. L.; Kim, S.; Azam, M. S.; Zeng, H.; Liu, Q.; Gibbs, J. M., pH-Dependent Inversion of Hofmeister Trends in the Water Structure of the Electrical Double Layer. *J. Phys. Chem. Lett.* **2017,** *8*, 2855-2861.
73. Darlington, A. M.; Jarisz, T. A.; DeWalt-Kerian, E. L.; Roy, S.; Kim, S.; Azam, M. S.; Hore, D. K.; Gibbs, J. M., Separating the pH-Dependent Behavior of Water in the Stern and Diffuse Layers with Varying Salt Concentration. *J. Phys. Chem. C* **2017,** *121*, 20229-20241.
74. Rehl, B.; Rashwan, M.; DeWalt-Kerian, E. L.; Jarisz, T. A.; Darlington, A. M.; Hore, D. K.; Gibbs, J. M., New Insights into χ(3) Measurements: Comparing Nonresonant Second Harmonic Generation and Resonant Sum Frequency Generation at the Silica/Aqueous Electrolyte Interface. *J. Phys. Chem. C* **2019,** *123* (17), 10991-11000.
75. Doğangün, M.; Ohno, P. E.; Liang, D.; McGeachy, A. C.; Bé, A. G.; Dalchand, N.; Li, T.; Cui, Q.; Geiger, F. M., Hydrogen-Bond Networks near Supported Lipid Bilayers from Vibrational Sum Frequency Generation Experiments and Atomistic Simulations. *J. Phys. Chem. B* **2018,** *122* (18), 4870-4879.
76. Yang, P.-K.; Huang, J. Y., Phase-Retrieval Problems in Infrared–Visible Sum-Frequency Generation Spectroscopy by the Maximum-Entropy Method. *J. Opt. Soc. Am. B* **1997,** *14* (10), 2443-2448.
77. Yang, P.-K.; Huang, J. Y., Model-Independent Maximum-Entropy Method for the Analysis of Sum-Frequency Vibrational Spectroscopy. *J. Opt. Soc. Am. B* **2000,** *17* (7), 1216-1222.

78. Sovago, M.; Vartiainen, E.; Bonn, M., Determining Absolute Molecular Orientation at Interfaces: A Phase Retrieval Approach for Sum Frequency Generation Spectroscopy. *J. Phys. Chem. C* **2009,** *113* (15), 6100-6106.
79. Sovago, M.; Vartiainen, E.; Bonn, M., Observation of Buried Water Molecules in Phospholipid Membranes by Surface Sum-Frequency Generation Spectroscopy. *J. Chem. Phys.* **2009,** *131* (16), 161107.
80. de Beer, A. G. F.; Samson, J.-S.; Hua, W.; Huang, Z.; Chen, X.; Allen, H. C.; Roke, S., Direct Comparison of Phase-Sensitive Vibrational Sum Frequency Generation with Maximum Entropy Method: Case Study of Water. *J. Chem. Phys.* **2011,** *135* (22), 224701.
81. de Beer, A. G. F.; Chen, Y.; Scheu, R.; Conboy, J. C.; Roke, S., Analysis of Complex Spectra Using Fourier Filtering. *J. Phys. Chem. C* **2013,** *117* (50), 26582-26587.
82. Roy, S.; Covert, P. A.; Jarisz, T. A.; Chan, C.; Hore, D. K., Surface–Bulk Vibrational Correlation Spectroscopy. *Anal. Chem.* **2016,** *88* (9), 4682-4691.
83. Yang, W.-C.; Hore, D. K., Broadband Models and Their Consequences on Line Shape Analysis in Vibrational Sum-Frequency Spectroscopy. *J. Chem. Phys.* **2018,** *149* (17), 174703.
84. Johansson, P. K.; Koelsch, P., Vibrational Sum-Frequency Scattering for Detailed Studies of Collagen Fibers in Aqueous Environments. *J. Am. Chem. Soc.* **2014,** *136* (39), 13598-13601.
85. Hofmann, M. J.; Koelsch, P., Retrieval of Complex χ(2) Parts for Quantitative Analysis of Sum-Frequency Generation Intensity Spectra. *J. Chem. Phys.* **2015,** *143* (13), 134112.
86. Bos, A. v. d., Alternative Interpretation of Maximum Entropy Spectral Analysis. *IEEE T. Inform. Theory* **1971,** *17* (4), 493-494.
87. Myalitsin, A.; Urashima, S.; Nihonyanagi, S.; Yamaguchi, S.; Tahara, T., Water Structure at the Buried Silica/Aqueous Interface Studied by Heterodyne-Detected Vibrational Sum-Frequency Generation. *J. Phys. Chem. C* **2016,** *120* (17), 9357-9363.
88. Ohno, P. E.; Chang, H.; Spencer, A. P.; Liu, Y.; Boamah, M. D.; Wang, H.-f.; Geiger, F. M., Beyond the Gouy–Chapman Model with Heterodyne-Detected Second Harmonic Generation. *J. Phys. Chem. Lett.* **2019,** *10* (10), 2328-2334.
89. Boamah, M. D.; Ohno, P. E.; Lozier, E.; Van Ardenne, J.; Geiger, F. M., Specifics about Specific Ion Adsorption from Heterodyne-Detected Second Harmonic Generation. *J. Phys. Chem. B* **2019,** *123* (27), 5848-5856.
90. Chang, H.; Ohno, P. E.; Liu, L.; Geiger, F. M., Direct Measurement of Charge Reversal on Lipid Bilayers using Heterodyne-Detected Second Harmonic Generation Spectroscopy. *J. Phys. Chem. B* **2020,** *124* (641-9).
91. Ma, E.; Ohno, P. E.; Kim, J.; Liu, Y.; Lozier, E. H.; Miller, T. F.; Wang, H.-F.; Geiger, F. M., A New Imaginary Term in the Second-Order Nonlinear Susceptibility from Charged Interfaces. *J. Phys. Chem. Lett.* **2021,** *12* (24), 5649-5659.
92. Ostroverkhov, V.; Waychunas, G. A.; Shen, Y. R., New Information on Water Interfacial Structure Revealed by Phase-Sensitive Surface Spectroscopy. *Phys. Rev. Lett.* **2005,** *94* (4), 046102.
93. Bakker, H. J.; Skinner, J. L., Vibrational Spectroscopy as a Probe of Structure and Dynamics in Liquid Water. *Chem. Rev.* **2010,** *110*, 1498-1517.
94. Lawrence, C. P.; Skinner, J. L., Ultrafast Infrared Spectroscopy Probes Hydrogen-Bonding Dynamics in Liquid Water. *Chem. Phys. Lett.* **2003,** *369* (3), 472-477.
95. Dalchand, N.; Dogangun, M.; Ohno, P. E.; Ma, E.; Martinson, A. B. F.; Geiger, F. M., Perturbation of Hydrogen Bonding Networks over Supported Lipid Bilayers by Poly(Allylamine Hydrochloride). *J. Phys. Chem. B* **2019,** *123* (19), 4251-4257.
96. Hore, D. K.; Tyrode, E., Probing Charged Aqueous Interfaces Near Critical Angles: Effect of Varying Coherence Length. *J. Phys. Chem. C* **2019,** *123* (27), 16911-16920.

97. Wang, H.; Xu, Q.; Liu, Z.; Tang, Y.; Wei, G.; Shen, Y. R.; Liu, W.-T., Gate-Controlled Sum-Frequency Vibrational Spectroscopy for Probing Charged Oxide/Water Interfaces. *J. Phys. Chem. Lett.* **2019,** *10*, 5943.
98. Paesani, F.; Voth, G. A., The Properties of Water: Insights from Quantum Simulations. *J. Phys. Chem. B* **2009,** *113* (17), 5702-5719.
99. Urashima, S.-h.; Myalitsin, A.; Nihonyanagi, S.; Tahara, T., The Topmost Water Structure at a Charged Silica/Aqueous Interface Revealed by Heterodyne-Detected Vibrational Sum Frequency Generation Spectroscopy. *J. Phys. Chem. Lett.* **2018,** *9* (14), 4109-4114.
100. Bischoff, M.; Biriukov, D.; Předota, M.; Marchioro, A., Second Harmonic Scattering Reveals Ion-Specific Effects at the SiO2 and TiO2 Nanoparticle/Aqueous Interface. *J. Phys. Chem. C* **2021,** *125* (45), 25261-25274.
101. Tuladhar, A.; Dewan, S.; Pezzotti, S.; Brigiano, F. S.; Creazzo, F.; Gaigeot, M.-P.; Borguet, E., Ions Tune Interfacial Water Structure and Modulate Hydrophobic Interactions at Silica Surfaces. *J. Am. Chem. Soc.* **2020,** *142* (15), 6991-7000.
102. Diot, J. L.; Joseph, J.; Martin, J. R.; Clechet, P., pH Dependence of the Si/SiO2 Interface State Density for EOS Systems: Quasi-Static and AC Conductance Methods. *J. Electroanal. Chem.* **1985,** *193*, 75-88.
103. Bousse, L.; De Rooij, N. F.; Bergveld, P., Operation of Chemically Sensitive Field-Effect Sensors As a Function of the Insulator-Electrolyte Interface. *IEEE Trans. Electron Devices* **1983,** *ED-30*, 1263-70.
104. Bard, A. J.; Faulkner, L. R., *Electrochemical Methods: Fundamentals and Applications, 2nd Edition*. John Wiley & Sons, Incorporated: 2000.
105. Azam, M. S.; Cai, C.; Gibbs, J. M.; Tyrode, E.; Hore, D. K., Silica Surface Charge Enhancement at Elevated Temperatures Revealed by Interfacial Water Signals. *J. Am. Chem. Soc.* **2020,** *142* (2), 669-673.
106. Lyklema, J., Overcharging, Charge Reversal: Chemistry or Physics? *Colloids Surf. A Physicochem. Eng.* **2006,** *291* (1), 3-12.
107. de Vos, W. M.; Lindhoud, S., Overcharging and Charge Inversion: Finding the Correct Explanation(s). *Adv. Colloid Interface Sci.* **2019,** *274*, 102040.
108. Wang, Z.-Y.; Zhang, P.; Ma, Z., On the Physics of Both Surface Overcharging and Charge Reversal at Heterophase Interfaces. *Phys. Chem. Chem. Phys.* **2018,** *20* (6), 4118-4128.
109. Pfeiffer-Laplaud, M.; Gaigeot, M.-P., Adsorption of Singly Charged Ions at the Hydroxylated (0001) α-Quartz/Water Interface. *J. Phys. Chem. C* **2016,** *120* (9), 4866-4880.